1   **Kinetic Controlled Glass Transition Measurement of Organic Aerosol Thin**

2   **Films Using Broadband Dielectric Spectroscopy**

4   Yue Zhang[1,2,£], Shachi Katira[3], Andrew Lee[1,†], Andrew T. Lambe[2], Timothy B. Onasch[1,2], Wen

5   Xu[2], William A. Brooks[2], Manjula R. Canagaratna[2], Andrew Freedman[2], John T. Jayne[2], Doug R.

6   Worsnop[2], Paul Davidovits[1,*], David Chandler[3, §], Charles E. Kolb[2,*]

8   *1 Department of Chemistry, Boston College, Chestnut Hill, MA, 02459*

9   *2 Aerodyne Research Inc., Billerica, MA, 01821*

10   *3 Department of Chemistry, University of California, Berkeley, CA, 94720*

11   *£ Now at Department of Environmental Science and Engineering, Gillings School of*

12   *Global Public Health, University of North Carolina at Chapel Hill*

13   *† Now at Department of Chemistry, University of North Carolina at Chapel Hill*

14   *§Deceased April 2017*

21   **Corresponding authors:* Paul Davidovits, (617)552-3617, davidovi@bc.edu

22   Charles E. Kolb, (978)663-9500 x 290, kolb@aerodyne.com

Abstract

25 Glass transitions from liquid to semi-solid and solid phase states have important implications for

26 reactivity, growth, and cloud forming (cloud condensation nuclei and ice nucleation) capabilities

27 of secondary organic aerosols (SOA). The small size and relatively low mass concentration of

28 SOA in the atmosphere make it difficult to measure atmospheric SOA glass transitions using

29 conventional methods. To circumvent these difficulties, we have adapted a new technique for

30 measuring glass forming properties of atmospherically relevant organic aerosols. Aerosol

31 particles to be studied are deposited in the form of a thin film onto an interdigitated electrode

32 (IDE) using electrostatic precipitation. Dielectric spectroscopy provides dipole relaxation rates

33 for organic aerosols as a function of temperature (373 to 233K) that are used to calculate the

34 glass transition temperatures for several cooling rates. IDE-enabled broadband dielectric

35 spectroscopy (BDS) was successfully used to measure the kinetically controlled glass transition

36 temperatures of glycerol and citric acid aerosols with selected cooling rates. The glass transition

37 results agree well with available literature data for these two compounds. The results indicate

38 that the IDE-BDS method can provide accurate glass transition data for organic aerosols under

39 atmospheric conditions. The BDS data obtained with the IDE-BDS technique can be used to

40 characterize glass transitions for both simulated and ambient organic aerosols and to model their

41 climate effects.

42

Keywords

44 Broadband Dielectric Spectroscopy   Glass Transition   Organic Aerosols

45 Interdigitated Electrodes   Thin Films   Aerosol Climate Effects

1 Introduction

46

47   Aerosol particles have important climate and health effects because they can scatter

48 sunlight, form clouds by acting as the cloud condensation nuclei (CCN), alter visibility, and

49 affect human health (Hallquist et al., 2009; Jimenez et al., 2009). Recent studies have confirmed

50 that organic aerosols, which comprise approximately half of the total submicron aerosol mass in

51 the atmosphere, can change from liquid to glassy state at ambient humidity levels and

52 temperatures (Zobrist et al., 2008; Virtanen et al., 2010; Zhang et al., 2015). The effect of

53 temperature may be especially important when aerosol particles are lifted into the free

54 troposphere, where the temperature change can rapidly alter their phase from liquid to glass

55 (Koop et al., 2011). The physical state of the aerosol strongly influences air quality and aerosol

56 climate effects. Evidence suggests that secondary organic aerosols, formed through oxidation of

57 gas phase organic compounds, have much lower vaporization rates than previously assumed,

58 which changes the reactivity of the gas phase species as well as their fate in the atmosphere. For

59 example, in the glassy state, the water vapor uptake by the SOA is greatly reduced, limiting the

60 ability of particles to nucleate liquid water and thus hampering the formation of liquid cloud

61 droplets (Shiraiwa et al., 2011). However, there is evidence that glassy SOAs are effective ice

62 nucleation agents. Their ability to nucleate ice crystals to form Cirrus clouds in the upper

63 troposphere may be particularly important given the key role of these clouds in global warming

64 (Wilson et al., 2012; Berkemeier et al., 2014). Lack of adequate data describing these processes

65 contribute to the high uncertainty of atmospheric aerosol impact on climate change (Shiraiwa et

66 al., 2017).

67   The importance of organic aerosols phase state in the evaluation of their climate effects

68 has motivated several studies in this field. However, these studies are difficult to perform and the

69   data obtained so far are limited. Renbaum-Wolff et al. (2013) studied the phase state and

70   viscosity of the water-soluble part of α-pinene SOA at several humidity levels and phase

71   separation effects. Zhang et al. (2015) characterized the viscosity of α-pinene SOA across a wide

72   range of RHs. Rothfuss and Petters (2017) studied the viscosities of various types of SOAs up to

73   10^6 Pa under sub-freezing temperature regimes. There have also been a few studies exploring the

74   glass transition temperature of atmospherically relevant organic compounds by using differential

75   scanning calorimetry (Koop et al., 2011; Dette et al., 2014).

76   Despite past studies, very little information is available on how organic aerosols become

77   glass as temperature, the rate of cooling, and heating changes. Such information is required to

78   model the aerosol phase when aerosols are transported from one region of the atmosphere to

79   another (Murray et al., 2010; Wilson et al., 2012). In an early 2011 study Koop and co-workers

80   performed experiments that led them to estimate glass transition temperature (T_g) values of 268-

81   290K for a range of surrogate biogenic SOA compounds by utilizing the differential scanning

82   calorimetry (DSC) method. The results show that oxidation and/or oligomerization reactions

83   leading to higher oxygen to carbon ratios (O:C), yielded higher T_g values. Dette et al. (2014)

84   used the "metastable aerosol by the low temperature evaporation of solvent" (MARBLES)

85   technique to provide information on the glass-to liquid transition temperatures of pure organic

86   compounds and organic-inorganic binary mixtures. Their results show that the glass transition

87   temperatures of these mixtures can be accurately described by the Gordon-Taylor equation, the

88   equation describing the glass transition of binary mixtures. However, to evaluate the impact of

89   SOA and its possible phase transitions on climate and air quality issues, the current techniques

90   need to be improved in order to adapt to the atmospheric aerosol sampling requirements.

91   The small particle size and relatively low concentration of SOA in the atmosphere make

92   it difficult to measure atmospheric SOA glass transitions using conventional methods. First, a

93   reliable measurement of glass transitions with currently used techniques requires a relatively

94   large mass, typically milligram levels of the compound, while reasonable field collection

95   methods yield organic aerosols in the femtogram mass range (Dette et al., 2014; Dette and Koop,

96   2015). Second, it is difficult to collect suspended aerosols and transfer them to the analysis

97   apparatus without contaminating the sample with trace water. Trace amounts of water absorbed

98   by SOA can substantially alter glass transition properties (Bateman et al., 2015; Price et al.,

99   2015; Rothfuss and Petters, 2017; Shiraiwa et al., 2017). To circumvent these difficulties, we

100   have adapted a new technique for measuring glass forming properties of atmospherically relevant

101   organic compounds. The technique combines broadband dielectric spectroscopy (BDS) utilizing

102   interdigitated electrodes (IDE) (Chen et al., 2012) with organic aerosol sample deposition using

103   electrostatic precipitation (Liu et al., 2013).

104   BDS is one of the most widely used techniques for measuring the dynamics and glass

105   transition of liquid and semi-solids (Dette et al., 2014; Richert, 2014). In the usual arrangement,

106   dielectric spectroscopy instruments consist of two parallel metallic plates with the sample filling

107   the space between the plates. As was stated, the traditional dielectric method usually requires

108   mass in the milligram range to perform the measurement (Richert, 2014). Such high mass

109   loading cannot be reasonably attained with aerosol collected under normal atmospheric

110   conditions. A relatively new technique, using interdigitated electrodes (IDE), which requires

111   only one surface for samples and requires mass only in the femtogram range (Chen et al., 2012),

112   is suitable for atmospheric aerosol phase studies. A thin film is deposited on the IDE first, then

113   the dielectric spectra are recorded to characterize the glass transition of aerosol particles at

114   variable cooling or heating rates.

115   The purpose of this study is to demonstrate the new IDE-BDS analysis technique by

116   presenting results of SOA surrogates glass transition studies using this technique. In section 2

117   below, we first describe the experimental setup including aerosol generation, thin film deposition

118   on the IDE, temperature conditioning chamber, and the BDS measurement system. Then data

119   analysis, including glass transition determination, is discussed in section 3. Section 4 includes

120   discussion of the advantages of the IDE-BDS method, as well as caveats associated with its

121   current implementation.

122   **2. Experimental Setup**

123   A schematic diagram of the experimental setup is shown in Figure 1. The setup is

124   conveniently divided into four parts:1. Aerosol sample generation, 2. Thin film formation via

125   electrostatic precipitation on the Interdigitated electrodes (IDE) with associated humidity control

126   3. Temperature conditioning chamber and 4. Broadband Dielectric Spectroscopy measurement

127   system.

128   **2.1 Aerosol generation.**

129   Two types of aerosol generation systems are used in our experiments. The first is a home-

130   made self-nucleation generation device used for producing liquid glycerol aerosol samples.

131   About 0.5 gram of the glycerol is placed at the bottom of a round flask and the temperature of the

132   flask is heated to 20°C below the boiling temperature of the organic liquid. A condenser is

133   connected to the top of the flask to cool the temperature of that region. A flow of 2 liters per

134   minute (Lpm) flow dry air passes through the condenser and brings the aerosol particles to the

135   region where the aerosols are precipitated onto the IDE.

136   The second method utilizes a commercial unit (TSI, 3076) to generate atomized citric

137   acid aerosols. About 0.5 gram of citric acid is dissolved in 100 mL of high purity water to form

138   the atomizing solution. About 30 psi pressure of dry air is applied on one end of the atomizer to

139   generate a constant 3 Lpm aerosol-containing flow to the second part of the system, which is the

140   thin film generation system that will be described below.

141   2.2 Interdigitated electrode (IDE) and thin film formation.

142   An IDE (NIB003744, MS-01/60, NETZSCH Instrument North America) is used in this

143   study as a substrate for measuring the dielectric constants of organic materials. The IDE consists

144   of two thin electrodes that are interdigitated together like entwined finger tips, as shown in

145   Figure 2. Each interdigitated pair serves as a small capacitor for dielectric analysis. The thin

146   electrodes are made from platinum (Pt) and are arrayed on a quartz substrate. The electrodes

147   utilized in this study are spaced 1 μm apart and are able to withstand temperatures up to 200 °C.

148   The combination of multiple interdigitated pairs of electrodes greatly enhances the sensitivity of

149   the technique compared to a single pair of electrodes that would have been used.

150   An electrostatic deposition method is used to deposit organic films on the IDE (Liu et al.,

151   2013). The electrostatic precipitator has one inlet and one outlet. A stream of aerosolized

152   oxygenated organic liquid droplets to be studied is passed through an inlet with a high voltage

153   corona discharger (-5000V) so that all the droplets are negatively charged to varying degrees.

154   The flow is directed above the substrate held at +3000 V within the precipitator. Due to opposite

155   charges, the charged particles are electrostatically deposited onto the substrate, gradually

156   merging together to form thin films. The remaining flow is then withdrawn from the precipitator

157   and flows through a HEPA filter connected to a pump. The flow rate through the precipitator is

158   maintained between 1.7-1.9 Lpm. Depending on the amount of aerosols being deposited onto the

159   surface, the deposition can remain either remain as discrete aerosol droplets, or at higher droplet

160   depositions, can form a uniform thin film, as shown in Figure 2.

2.3 Temperature conditioning chamber.

161

162   The IDE substrate coated with organic material is then transported to the temperature

163 conditioning chamber using a tweezer. The temperature conditioning chamber consists of a

164 stainless steel cap and a heating/cooling surface using either a liquid nitrogen cooler or a heating

165 furnace. The sample temperature can be controlled from ~-150°C to +200°C. Details of the

166 chamber are shown in Figure 1. The cooling rate can be varied from 1 K/min to 25 K/min. The

167 chamber is flushed with dry nitrogen gas to reduce the relative humidity (RH) prior to

168 temperature conditioning. A K type thermocouple is located on top of a reference cell inside the

169 conditioning chamber, to monitor sample temperature. The typical cooling cycle starts around 20

170 °C and ends at about -140 °C, while the heating cycle starts at -140 °C and ends at 30 °C. The

171 cooling and heating cycle are adjusted with the desired cooling/heating rates between 2 K/min

172 and 10 K/min.

173 **2.4 Broadband Dielectric Spectroscopy (BDS) measurement system.**

174   The BDS instrument used in this study is manufactured by NETZSCH Inc. (DEA 288

175 model). A periodic signal from the instrument is applied to the IDE electrodes. The frequency of

176 the signal ranges from 10^{-3} Hz to 1 MHz. The data acquisition part of the instrument then

177 measures the impedance, Z_{sample}, of the sample as a function of the applied frequency. The

178 impedance measurement yields the capacitance of the sample on top of the IDE. By measuring

179 the impedance of the uncoated and organic-coated IDE, three IDE capacitances can be obtained,

180 i.e., when the IDE is uncoated Z_{empty}, when it is coated with organic compounds, Z_{coated}, and the

181 geometric capacitance of the IDE without any substrate, Z_{geo}. Approximate values of the real and

182 imaginary part of the sample permittivity, ε_{sample}, can be obtained using Eq. (1) (Chen et al.,

183 2012)

184
$$\varepsilon_{sample} = 1 + \frac{Z_{loaded} - Z_{empty}}{Z_{geo}} \qquad (1)$$

185   For demonstration and data comparison purposes, we have used glycerol (99%, Sigma

186   Aldrich, St. Louis, MO, USA) as the test compound for homogeneous nucleation and citric acid

187   (99%, Sigma Aldrich, St. Louis, MO, USA) as the surrogate organic aerosol generated by

188   atomizing solutions. For atomizing solutions, the surrogate compound is mixed with high purity

189   water. All reagents were used as provided without further purification.

190   **3. Data Analysis**

191   **3.1 Calculating Relaxation Time τ**

192   The thin film on the IDE is usually cooled at a selected cooling rate and then heated back to 30

193   °C. After a cooling-heating cycle, the dielectric constant at each temperature measured, $\varepsilon\ (\omega)$, is

194   recorded by instrument. The relaxation time, τ, can be obtained by curve fitting the Havriliak-

195   Negami equation of the real and imaginary parts ($\varepsilon'(\omega)$ and $\varepsilon''(\omega)$, respectively) with the

196   frequency ω, as shown in Figure 3 and S1 (Chen et al., 2012). The detailed equation of $\varepsilon'(\omega)$

197   and $\varepsilon''(\omega)$ are shown in Eqns. (S1) and (2). At each temperature, the dielectric spectra often

198   show peaks at specific frequencies, designated as dielectric relaxation peaks. Different peaks

199   give different τ values after fitting Eq. (2) into the data points.

200     $$\varepsilon''(\omega) = \Delta\varepsilon(1 + 2(\omega\tau)^{\alpha} \cos\left(\frac{\pi\alpha}{2}\right) + (\omega\tau)^{2\alpha})^{-\beta/2} \sin(\beta\varphi) \qquad (2)$$

201   with $\Delta\varepsilon = \varepsilon_s - \varepsilon_\infty$, $\varphi = \arctan\left(\frac{(\omega\tau)^{\alpha} \sin\left(\frac{\pi\alpha}{2}\right)}{1 + (\omega\tau)^{\alpha} \cos\left(\frac{\pi\alpha}{2}\right)}\right)$

202   where ε_s is the permittivity at lower frequency, ε_∞ is the permittivity at the high frequency limit,

203   α, β are fitting parameters, and τ is the characteristic relaxation time of the medium

204   (Adrjanowicz et al., 2009; Chen et al., 2012).

205   Log τ is then plotted as a function of the invert of the temperature to further examine how

206   relaxation time changes as a function of temperature. The error bar represents twice the standard

207   deviation of the fitting result. The resulting curve can be used to calculate the glass transition

208   temperature of the compound, as described in section 3.2.

209   **3.2 Glass Transition Determination**

210   The glass transition temperature is defined as the temperature where a compound changes

211   from liquid to glass. Several methods have been used to indirectly determine the glass transition

212   temperatures. A common way to calculate the glass transition temperature using BDS is to

213   measure relevant parameters and to calculate the dielectric relaxation τ described in section 3.1

214   at several equilibrium temperatures T, and then plot log τ as a function of 1000/T. The data points

215   are fitted by using Vogel-Fulcher-Tammann (VFT) formula (Vogel, 1921; Fulcher, 1925;

216   Tammann and Hesse, 1926). The glass transition is customarily defined as the temperature where

217   τ =100 s in the fitted curve (Chen et al., 2012; Richert, 2014). The result usually agrees with the

218   differential scanning calorimetry (DSC) measurement within a few degrees (Richert, 2014).

219   However the method is limited, because not all compounds become glass as τ =100 s.

220   Furthermore, this method does not take into account kinetic effects on glass transition,

221   specifically the effect of cooling and heating rates (Elmatad et al., 2009, 2010; Keys et al., 2013;

222   Limmer and Chandler, 2014; Hudson, 2016), as glass transition temperature changes with

223   cooling and heating rates.

224   The following method, used in our studies, takes into account the effect of cooling rate on

225   the glass transition. As a compound is cooled and transitions from a liquid to a supercooled

226   liquid it exhibits super Arrhenius behavior described in Elmatad et al.(2009). As temperature

227   further decreases, the supercooled liquid becomes glass-like, which exhibits Arrhenius behavior.

228   The temperature where the supercooled liquid changes to glass is the glass transition temperature

229   of the compound at the specific cooling rate studied. As the sample is continuously cooled at a

230   specific cooling rate, the dielectric relaxation peaks can be generated as a function of the sample

231   temperature. The experimentally obtained data are plotted in the form $\log \tau$ vs 1/T. The data

232   obtained at the higher temperature range are fitted to the super-Arrhenius function and the data

233   obtained at the lower temperature range are fitted to the Arrhenius function. As shown in Figure

234   4, the kinetically controlled glass transition temperature (or the true glass transition temperature)

235   is the temperature at the intercept of the two functions. The traditional method determines the

236   glass transition temperature as shown in dashed lines where $\tau = 100$ s. Depending on the

237   compound, the true glass transition temperature may not be the same as the glass transition

238   temperature determined by using $\tau = 100$ s, as shown in section 4 below. The error bar of the

239   glass transition temperature is estimated based on varying the fitting parameters of the super

240   Arrhenius curve and Arrhenius line within a one-sigma range.

241   For glycerol, measurements of glass transitions were performed at three cooling rates: 2

242   K/min, 5 K/min, and 10 K/min. At each cooling rate the compound is cooled from approximately

243   300 K to 125 K, while the dielectric peaks are measured simultaneously as a function of

244   temperature. The organic film is thin enough so that its temperature reaches equilibrium with the

245   cooling/heating medium, reducing the errors caused by heat transfer within the sample itself.

246   Such measurements are difficult to perform with conventional techniques due to slow heat

247   transfer in large mass samples, which often leads to inaccurate results. The effect of cooling rates

248   on glass transition measurements will be discussed in the following section.

4 Results and Discussion

4.1 Glass transition temperature of selected organic compounds

249

250

251   Aerosols are generated by two methods in this study, and in each method, we measured

252   the glass transition of a compound that has been studied in the literature. Glycerol and citric acid

253   particles were generated through the homogeneous nucleation method and atomizer method,

254   respectively. The measured dielectric spectra of glycerol and citric acid show distinct dielectric

255   relaxation rates at different frequencies as the temperature changes. This is a confirmation of the

256   expected behavior.

257   As is shown in Table 1, our kinetically controlled glass transition data agree well with

258   previously measured literature values of glycerol (Zondervan et al., 2007; Chen et al., 2012;

259   Amann-Winkel et al., 2013). For citric acid, our kinetically controlled glass transition result

260   fitted using Eq. (S2) agrees reasonably well (within 10% error) with two literature results (Lu

261   and Zografi, 1997; Bodsworth et al., 2010). The third literature data (Murray, 2008) is based on

262   extrapolation of experimental fitting result and is about 16% lower than the value obtained from

263   this study. The differences can be explained by the following reasons: (1) As described above,

264   our method measured the kinetically controlled glass transition temperature at a given cooling

265   rate, i.e., the transition of the long range intermolecular movements of the sample to determine

266   the glass transition temperature. If the more conventional method, i.e. fitting the super-Arrhenius

267   curve to obtain the glass transition temperature when $\tau=100$ s, is applied to the data, as shown in

268   Figure 5, the obtained glass transition temperature would be 281 ± 3 K, which is within 1%

269   difference compared with the two nearest literature values. Therefore, the difference herein is

270   due to including the kinetically controlled process in glass transition. Based on the theory

271   described by Chandler and co-authors (Elmatad et al., 2009; Keys et al., 2013; Hudson, 2016),

272   we report the citric acid glass transition temperature as 307 ± 5 K at 5 K/min cooling rate, which

273   we believe is a more accurate way of reflecting the glass transition process, as the kinetical

274   process is considered. The relevant data plot is shown in Figure 5. (2) Moreover, glass transition

275   data of citric acid are rather limited and there are differences between each study. For instance,

276   from the literature data, the differences between three reported glass transition temperatures are

277   up to 10%, which is the same value comparing our data to the other two nearest literature results.

278   Even though the reasons listed above are likely to be the primary reasons leading to

279   ~10% difference of the glass transition temperature of citric acid between our data and the

280   literature, the following factors may play a role: (1) Atomizing the citric acid solution and re-

281   depositing citric particles via electrostatic precipitation could introduce impurities during the

282   atomization process the may affect the glass transition temperatures; (2) The glass transition of

283   citric acid was measured during a warming cycle. A fast non-recordable cooling cycle at

284   20K/min was performed prior to warming in order to inhibit the citric acid crystal formation. The

285   hysteresis effect will lead to an increase of the glass transition temperature from the warming

286   cycle compared with data obtained from the cooling cycle (Wang et al., 2011); (3) Lu and

287   Zogrfai (1997) have shown that different ways of preparing the citric acid can lead to differences

288   in glass transition measurements. The thicknesses of the thin films are equal to or less than one

289   micrometer, leading to confinement effects and differences in glass transition temperature

290   measured from bulk compounds (Park and McKenna, 2000). The results show that the thin film

291   IDE-BDS method can accurately measure the glass transition temperatures of various organic

292   compounds that are comparable to the composition of organic aerosols.

4.2 The influence of cooling rates on glass transition temperatures

293

294   One advantage of this study is the introduction of cooling and heating rates as variables

295   for glass transition temperature measurement for organic compounds. For BDS studies, a glass

296   transition temperature of a compound is often deduced by measuring the sample at a few

297   isothermal temperatures and fitting the curve of temperature and relaxation time in order to

298   identify the temperature when relaxation time corresponds to 100 s. The transitional approach

299   makes it difficult to directly compare the result with glass transition temperatures deduced from

300   DSC studies with variable cooling rates. One of the advantages of our technique is that variable

301   cooling rate measurements are performed on the thin film and the cooling rate dependent glass

302   transition temperature of glycerol is determined.

303   The influence of cooling rate on glass transition temperature was carefully examined by

304   repeating the glycerol experiment at two additional cooling rates. The resulting super Arrhenius

305   curve for each cooling rate is plotted against the Arrhenius lines of that cooling rate, as shown in

306   Figure 6. As a compound remains in the supercooled liquid stage, the relaxation time is short

307   enough that it is constantly in equilibrium with external perturbations, leading the super-

308   Arrhenius region totally reversible so it should behave the same for all cooling rates. The super

309   Arrhenius part of the data from all three different cooling rates all collapse into one single trend,

310   indicating the data collected agree well with the theory. Reference data from Elmatad et al.

311   (2009) is also plotted as the black dash line and it also agrees well with our experimental results.

312   As the cooling continues, the relaxation time gets longer until it cannot keep up with the external

313   temperature change, leading to the compound falling out equilibrium and forming a glass.

314   Therefore, a faster cooling rate often leads to a quick falling out of equilibrium and a higher glass

315   transition temperature for the compounds studied, as demonstrated in Figure 6. Based on the

316   intercept of the super-Arrhenius curve and the Arrhenius line, the glass transition temperatures

317   for 5 K/min and 10 K/min cooling are determined to be 192 ± 2 K and 194 ± 2 K. For 2 K/min

318   cooling, because an Arrhenius line does not appear within our range of measurement, the glass

319   transition temperature will likely be lower than 189 K.

320   Our results agree reasonably well with other studies for the glass transition temperatures

321   of glycerol and citric acid. However, there are a couple possible caveats for this study. One is

322   the influence of humidity during the cooling process. Even though dry nitrogen is used to flush

323   through the cooling chamber to remove any extra water vapor present prior to cooling, there is

324   still the possibility that the chamber wall surface can degas and release water vapor to the system

325   during the cooling process. The effect of water vapor on the testing materials is likely to be small,

326   but should be considered when the organic compound tested can readily absorb water at low RH

327   conditions. The other potential caveat is the influence of non-equilibrium heat transfer within the

328   thin film on glass transition temperature measurement. Because the sample is being cooled from

329   underneath, the heat transfer between the upper and lower boundaries of the film can lead to

330   uncertainties of the glass transition temperature. The organic thin films made during the

331   experiments are within the micrometer range, therefore the thermal gradient between is small

332   enough to be likely insignificant compared with other systematic errors. Moreover, theoretical

333   models to predict the glass transition of compounds with variable cooling rates are needed in

334   further studies to verify and explain these experimental measurements.

335   **5 Summary**

336   In this work, we have demonstrated a novel method using interdigitated electrodes,

337   broadband dielectric spectroscopy, and electrostatic precipitation together as an efficient and

338   powerful approach studying the phase and glass transitions of organic particles under various

339   cooling rates. The method is particularly suitable for studying the glass transition of submicron

340   organic particles whose mass loading is generally too small for other kinds of glass transition

341   measurement techniques. The results from this technique agree well with published studies using

342   other methods. Future publications will report glass transition measurements for simulated SOA

343   mixtures as well as laboratory produced SOA particles.

344   The dielectric relaxation peaks of glycerol and citric acid were recorded and the

345   logarithm of characteristic relaxation time were calculated and plotted as a function of inverse

346   temperature. The super Arrhenius and Arrhenius fittings were used to determine the temperature

347   where the super-cooled liquid fell out of equilibrium to become glass, which is defined at the

348   experimental true glass transition temperature. Furthermore, cooling rates are demonstrated to

349   have an effect on the glass transition temperature. By changing the cooling rate from 2 K/min to

350   10 K/min, the glass transition temperature increases by at least 5 K for glycerol.

351   **Acknowledgments** We acknowledge James Brogan, Yatish Parmar, Professor Ranko Richert,

352   Lindsay Renbaum-Wolff, Wade Robinson, Paul Kebabian, Professor Andrew Ault for useful

353   discussions and assistance with the experiments.

354   **Funding** This material is based upon work supported by the National Science Foundation

355   Environmental Chemistry Program in the Division of Chemistry under Grant No. 1506768, No.

356   1507673, and No. 1507642.

357   **Competing financial interests:** The authors declare no competing financial interests.

Table 1. Glass transition temperatures for glycerol and citric acid measured by broadband

dielectric spectroscopy with thin film interdigitated electrode array

Compound	Chemical Formula	T_g (K)-Measured	T_g (K)-Literature
Glycerol	$C_3H_8O_3$	<189 K (2 K/min)	190 K (Zondervan et al., 2007)
		192 ± 2 K (5 K/min)	191 K (Chen et al., 2012)
		194 ± 2 K (10 K/min)	196 K (Amann-Winkel et al., 2013)
Citric Acid	$C_6H_8O_7$	307 ± 5 K (5 K/min)	281 ± 5 K (Bodsworth et al., 2010)[*]
			285 ± 0.2 K (Lu and Zografi, 1997)
			260 ± 10 K (Murray, 2008)[**]

[*] The data was based on modeling result.   [**]The data was based on fitting extrapolation result.

List of Figures
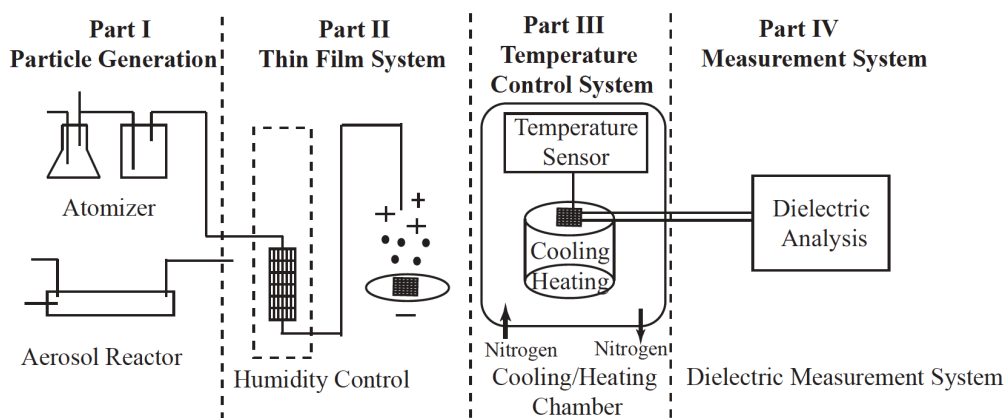
Figure 1. A schematic diagram of the experimental setup and procedure. The experimental

approach consists of four parts: aerosol generation, thin film deposition using an

electrostatic precipitator, the temperature control system, and the broadband dielectric

spectroscopy measurement system.
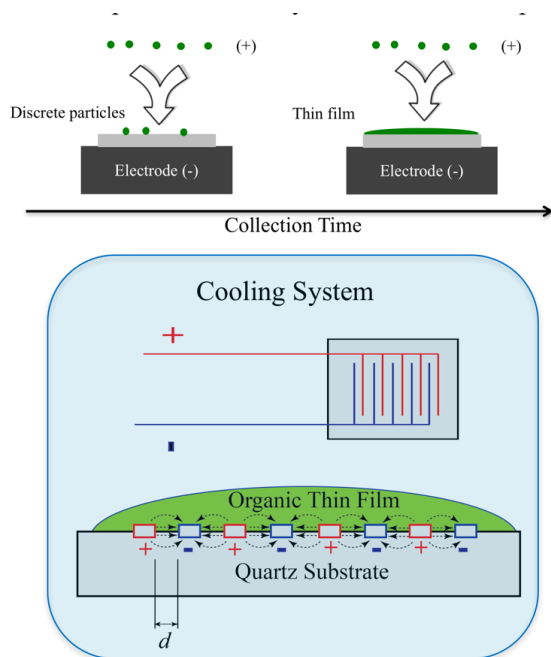
Figure 2. A schematic diagram of the key experimental setup. The upper panel shows the formation of organic thin films though electrostatic deposition. The lower panel shows the working principle of broadband dielectric spectroscopy (BDS) with an interdigitated electrode sensor. A compound is placed on an array of interdigitated electrodes with a periodic voltage, and the compound's impedance is recorded.
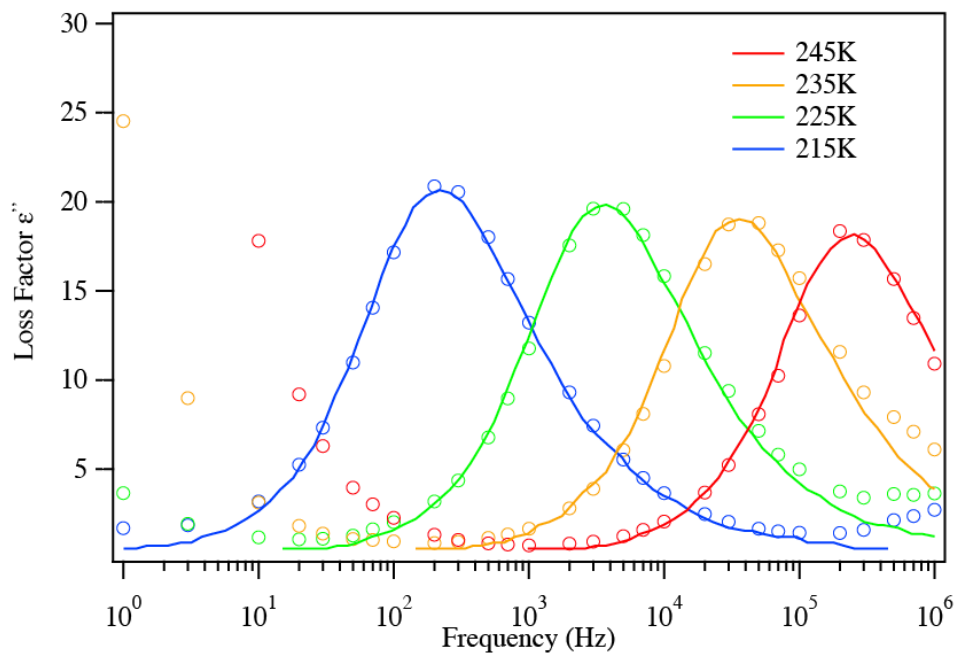
Figure 3. The dielectric relaxation spectrum of glycerol at different temperatures. The open

circles are measurement experimental data and the solid lines are literature data from

Chen et al. (2012). As temperature decreases, the dielectric peaks shift towards lower

frequencies, indicating the relaxation timescale increases.
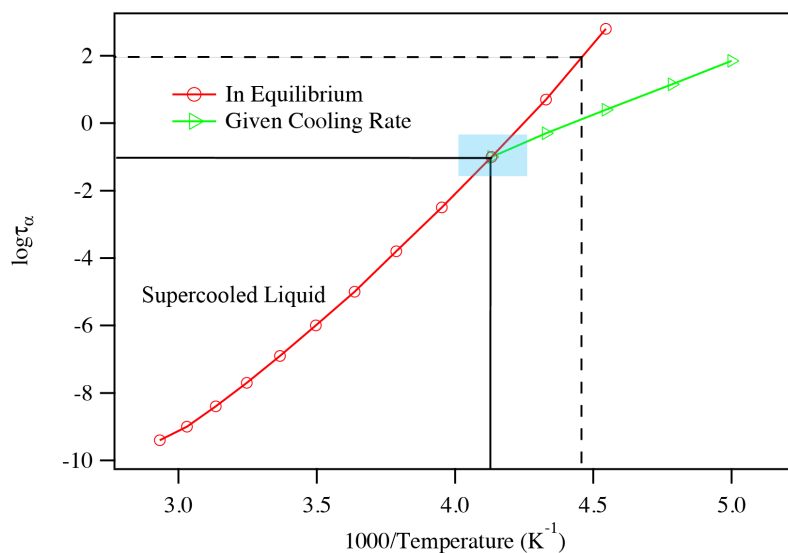
Figure 4. The logarithm of the relaxation is plotted against inverse T, i.e., log τ vs 1000/T. By linking the data points together, one can plot the super-Arrhenius curve (red) vs. the Arrhenius line (green). Using a consistent cooling rate, the intersection of the two regions identifies the compound's glass transition temperature, as indicated by the shaded blue region. The intersection of the two black lines represents the glass transition point. The intersection of the two black dashed lines shows the glass transition temperature determined using traditional method when τ=100 s.
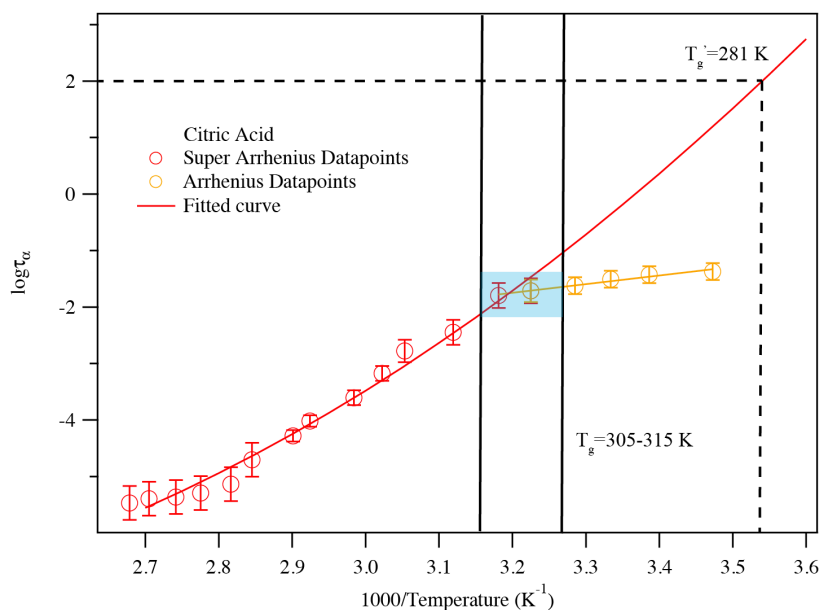
Figure 5. A plot of superimposed datapoints and curves constructed for citric acid warmed at

5K/min. The solid color lines represent the fitted curves for the super Arrhenius and Arrhenius

region. The blue shaded area shows the glass transition region. The two vertical black lines

associated with the blue shaded area indicate the corresponding temperature range where the

super Arrhenius curve intersects with the Arrhenius line. The intersect between the two black

dashed lines indicate the glass transition temperature determined using traditional method when

τ=100 s.
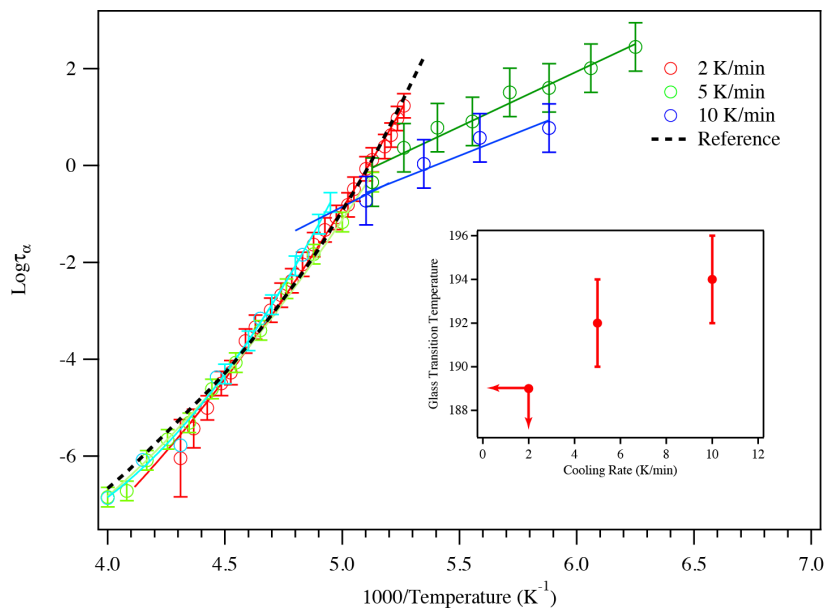
Figure 6. A plot of superimposed datapoints and curves constructed for glycerol cooled at 2K/min, 5K/min, and 10K/min. The black dashed line represents the literature data of the super-Arrhenius region from Elmatad et al. The open circles are experimental data and the solid lines are fitting results. The inset shows the glass transition temperature of glycerol as a function of cooling rates. At 2 K/min cooling, the glass transition temperature has a higher bound of 189 K.

References

Adrjanowicz, K., Wojnarowska, Z., Wlodarczyk, P., Kaminski, K., Paluch, M., and Mazgalski, J.: Molecular mobility in liquid and glassy states of Telmisartan (TEL) studied by Broadband Dielectric Spectroscopy, Eur. J. Pharm. Sci., 38, 395-404, https://doi.org/10.1016/j.ejps.2009.09.009, 2009.

Amann-Winkel, K., Gainaru, C., Handle, P. H., Seidl, M., Nelson, H., Böhmer, R., and Loerting, T.: Water's second glass transition, Proc. Natl. Acad. Sci. USA, 110, 17720-17725, 10.1073/pnas.1311718110, 2013.

Bateman, A. P., Bertram, A. K., and Martin, S. T.: Hygroscopic Influence on the Semisolid-to-Liquid Transition of Secondary Organic Materials, J. Phys. Chem. A, 119, 4386-4395, 10.1021/jp508521c, 2015.

Berkemeier, T., Shiraiwa, M., Pöschl, U., and Koop, T.: Competition between water uptake and ice nucleation by glassy organic aerosol particles, Atmos. Chem. Phys., 14, 12513-12531, 10.5194/acp-14-12513-2014, 2014.

Bodsworth, A., Zobrist, B., and Bertram, A. K.: Inhibition of efflorescence in mixed organic-inorganic particles at temperatures less than 250 K, Phys. Chem. Chem. Phys., 12, 12259-12266, 10.1039/C0CP00572J, 2010.

Chen, Z., Sepúlveda, A., Ediger, M. D., and Richert, R.: Dielectric spectroscopy of thin films by dual-channel impedance measurements on differential interdigitated electrode arrays, Eur. Phys. J. B, 85, 1-5, 10.1140/epjb/e2012-30363-0, 2012.

Dette, H. P., Qi, M., Schröder, D. C., Godt, A., and Koop, T.: Glass-Forming Properties of 3-Methylbutane-1,2,3-tricarboxylic Acid and Its Mixtures with Water and Pinonic Acid, J. Phys. Chem. A, 118, 7024-7033, 10.1021/jp505910w, 2014.

Dette, H. P., and Koop, T.: Glass Formation Processes in Mixed Inorganic/Organic Aerosol Particles, J. Phys. Chem. A, 119, 4552-4561, 10.1021/jp5106967, 2015.

Elmatad, Y. S., Chandler, D., and Garrahan, J. P.: Corresponding States of Structural Glass Formers, J. Phys. Chem. B., 113, 5563-5567, 10.1021/jp810362g, 2009.

Elmatad, Y. S., Chandler, D., and Garrahan, J. P.: Corresponding States of Structural Glass Formers. II, The Journal of Physical Chemistry B, 114, 17113-17119, 10.1021/jp1076438, 2010.

Fulcher, G. S.: ANALYSIS OF RECENT MEASUREMENTS OF THE VISCOSITY OF GLASSES, J. Am. Ceram. Soc., 8, 339-355, 10.1111/j.1151-2916.1925.tb16731.x, 1925.

Hallquist, M., Wenger, J. C., Baltensperger, U., Rudich, Y., Simpson, D., Claeys, M., Dommen, J., Donahue, N. M., George, C., Goldstein, A. H., Hamilton, J. F., Herrmann, H., Hoffmann, T., Iinuma, Y., Jang, M., Jenkin, M. E., Jimenez, J. L., Kiendler-Scharr, A., Maenhaut, W., McFiggans, G., Mentel, T. F., Monod, A., Prévôt, A. S. H., Seinfeld, J. H., Surratt, J. D., Szmigielski, R., and Wildt, J.: The formation, properties and impact of secondary organic aerosol: current and emerging issues, Atmos. Chem. Phys., 9, 5155-5236, 10.5194/acp-9-5155-2009, 2009.

Hudson, A.: Statistical Mechanics and Dynamics of Liquids in and out of Equilibrium, Ph.D., University of California, Berkeley, 2016.

Jimenez, J. L., Canagaratna, M. R., Donahue, N. M., Prevot, A. S. H., Zhang, Q., Kroll, J. H., DeCarlo, P. F., Allan, J. D., Coe, H., Ng, N. L., Aiken, A. C., Docherty, K. S., Ulbrich, I. M., Grieshop, A. P., Robinson, A. L., Duplissy, J., Smith, J. D., Wilson, K. R., Lanz, V. A., Hueglin, C., Sun, Y. L., Tian, J., Laaksonen, A., Raatikainen, T., Rautiainen, J., Vaattovaara, P., Ehn, M., Kulmala, M., Tomlinson, J. M., Collins, D. R., Cubison, M. J., E, Dunlea, J., Huffman, J. A., Onasch, T. B., Alfarra, M. R., Williams, P. I., Bower, K., Kondo, Y., Schneider, J., Drewnick, F.,

Borrmann, S., Weimer, S., Demerjian, K., Salcedo, D., Cottrell, L., Griffin, R., Takami, A., Miyoshi, T., Hatakeyama, S., Shimono, A., Sun, J. Y., Zhang, Y. M., Dzepina, K., Kimmel, J. R., Sueper, D., Jayne, J. T., Herndon, S. C., Trimborn, A. M., Williams, L. R., Wood, E. C., Middlebrook, A. M., Kolb, C. E., Baltensperger, U., and Worsnop, D. R.: Evolution of organic aerosols in the atmosphere, Science, 326, 1525-1529, 2009.

Keys, A. S., Garrahan, J. P., and Chandler, D.: Calorimetric glass transition explained by hierarchical dynamic facilitation, Proc. Natl. Acad. Sci. USA, 110, 4482-4487, 10.1073/pnas.1302665110, 2013.

Koop, T., Bookhold, J., Shiraiwa, M., and Poschl, U.: Glass transition and phase state of organic compounds: dependency on molecular properties and implications for secondary organic aerosols in the atmosphere, Phys. Chem. Chem. Phys., 13, 19238-19255, 2011.

Limmer, D. T., and Chandler, D.: Theory of amorphous ices, Proceedings of the National Academy of Sciences of the United States of America, 111, 9413-9418, 10.1073/pnas.1407277111, 2014.

Liu, P., Zhang, Y., and Martin, S. T.: Complex refractive indices of thin films of secondary organic materials by spectroscopic ellipsometry from 220 to 1200 nm, Environ. Sci. Technol., 47, 13594-13601, 10.1021/es403411e, 2013.

Lu, Q., and Zografi, G.: Properties of citric acid at the glass transition, J. Pharm. Sci., 86, 1374-1378, 10.1021/js970157y, 1997.

Murray, B. J.: Inhibition of ice crystallisation in highly viscous aqueous organic acid droplets, Atmos. Chem. Phys., 8, 5423-5433, 10.5194/acp-8-5423-2008, 2008.

Murray, B. J., Wilson, T. W., Dobbie, S., Cui, Z., Al-Jumur, S. M. R. K., Mohler, O., Schnaiter, M., Wagner, R., Benz, S., Niemand, M., Saathoff, H., Ebert, V., Wagner, S., and Karcher, B.:

Heterogeneous nucleation of ice particles on glassy aerosols under cirrus conditions, Nature
Geosci, 3, 233-237, http://www.nature.com/ngeo/journal/v3/n4/suppinfo/ngeo817_S1.html,
2010.

Park, J.-Y., and McKenna, G. B.: Size and confinement effects on the glass transition behavior of
polystyrene/o-terphenyl polymer solutions, Physical Review B, 61, 6667-6676, 2000.

Price, H. C., Mattsson, J., Zhang, Y., Bertram, A., Davies, J. F., Grayson, J. W., Martin, S. T.,
O'Sullivan, D., Reid, J. P., Rickards, A. M. J., and Murray, B. J.: Water diffusion in
atmospherically relevant [small alpha]-pinene secondary organic material, Chemical Science,
10.1039/C5SC00685F, 2015.

Renbaum-Wolff, L., Grayson, J. W., Bateman, A. P., Kuwata, M., Sellier, M., Murray, B. J.,
Shilling, J. E., Martin, S. T., and Bertram, A. K.: Viscosity of α-pinene secondary organic
material and implications for particle growth and reactivity, Proc. Natl. Acad. Sci. USA, 110,
8014-8019, 10.1073/pnas.1219548110, 2013.

Richert, R.: Supercooled Liquids and Glasses by Dielectric Relaxation Spectroscopy, in: Adv.
Chem. Phys., John Wiley & Sons, Inc., 101-195, 2014.

Rothfuss, N. E., and Petters, M. D.: Characterization of the temperature and humidity-dependent
phase diagram of amorphous nanoscale organic aerosols, Phys. Chem. Chem. Phys., 19, 6532-
6545, 10.1039/C6CP08593H, 2017.

Shiraiwa, M., Ammann, M., Koop, T., and Pöschl, U.: Gas uptake and chemical aging of
semisolid organic aerosol particles, Proc. Natl. Acad. Sci. USA, 108, 11003-11008,
10.1073/pnas.1103045108, 2011.

Shiraiwa, M., Li, Y., Tsimpidi, A. P., Karydis, V. A., Berkemeier, T., Pandis, S. N., Lelieveld, J., Koop, T., and Pöschl, U.: Global distribution of particle phase state in atmospheric secondary organic aerosols, Nat. Commun., 8, 15002, 10.1038/ncomms15002

https://www.nature.com/articles/ncomms15002 - supplementary-information, 2017.

Tammann, G., and Hesse, W.: Die Abhängigkeit der Viscosität von der Temperatur bie unterkühlten Flüssigkeiten, Z. Anorg. Allg. Chem., 156, 245-257, 10.1002/zaac.19261560121, 1926.

Virtanen, A., Joutsensaari, J., Koop, T., Kannosto, J., Yli-Pirila, P., Leskinen, J., Makela, J. M., Holopainen, J. K., Poschl, U., Kulmala, M., Worsnop, D. R., and Laaksonen, A.: An amorphous solid state of biogenic secondary organic aerosol particles, Nature, 467, 824-827, 10.1038/nature09455, 2010.

Vogel, H.: The law of the relation between the viscosity of liquids and the temperature, Physikalische Zeitschrift, 22, 645, citeulike-article-id:4001983, 1921.

Wang, Y. Z., Li, Y., and Zhang, J. X.: Scaling of the hysteresis in the glass transition of glycerol with the temperature scanning rate, J. Chem. Phys., 134, 114510, 10.1063/1.3564919, 2011.

Wilson, T. W., Murray, B. J., Wagner, R., Möhler, O., Saathoff, H., Schnaiter, M., Skrotzki, J., Price, H. C., Malkin, T. L., Dobbie, S., and Al-Jumur, S. M. R. K.: Glassy aerosols with a range of compositions nucleate ice heterogeneously at cirrus temperatures, Atmos. Chem. Phys., 12, 8611-8632, 10.5194/acp-12-8611-2012, 2012.

Zhang, Y., Sanchez, M. S., Douet, C., Wang, Y., Bateman, A. P., Gong, Z., Kuwata, M., Renbaum-Wolff, L., Sato, B. B., Liu, P. F., Bertram, A. K., Geiger, F. M., and Martin, S. T.: Changing shapes and implied viscosities of suspended submicron particles, Atmos. Chem. Phys., 15, 7819-7829, 10.5194/acp-15-7819-2015, 2015.

Zobrist, B., Marcolli, C., Pedernera, D. A., and Koop, T.: Do atmospheric aerosols form glasses?, Atmos. Chem. Phys., 8, 5221-5244, 10.5194/acp-8-5221-2008, 2008.

Zondervan, R., Kulzer, F., Berkhout, G. C. G., and Orrit, M.: Local viscosity of supercooled glycerol near Tg probed by rotational diffusion of ensembles and single dye molecules, Proc. Natl. Acad. Sci. USA, 104, 12628-12633, 10.1073/pnas.0610521104, 2007.